JOURNAL OF THEORETICAL
AND APPLIED MECHANICS
3, 40, 2002

EXPERIMENT ON A CANTILEVER BEAM CONTROL AND THEORETICAL APPROXIMATION

MAREK PIETRZAKOWSKI

Institute of Machine Design Fundamentals, Warsaw University of Technology
e-mail: mpietrz@ipbm.simr.pw.edu.pl

The aim of this research is to investigate experimentally as well as numerically active damping effects of cantilever beam transverse vibrations. The control system under consideration consists of collocated piezoceramic sensor and actuator patches, which are coupled with velocity feedback. Experimental results of free and forced vibrations confirmed the effectiveness of the control circuit with the analog derivative controller for suppression of low-frequency beam motion. The numerical simulation is performed to verify the theoretical models of the tested mechanical system. The analysis is based on the simplified pure bending interaction between the perfectly bonded piezoactuator and the beam, which has a constant equivalent stiffness or is locally stiffened by the piezoceramic patches. The applied dynamic coupling model includes the effects of the actuator tangential inertia forces and the bonding layer with a finite shearing stiffness. The results of the simulation are in a good agreement with the experiment taking in the simplified model of the system. Considering the bonding layer and the actuator longitudinal movement decreases the active damping effectiveness even for a relatively stiff glue layer.

Key words: transverse vibrations, active damping, piezoelectric elements, experiment, simulation

1. Introduction

Piezoelectric materials such as lead zirconate titanate (PZT) ceramics and poly vinylidene fluoride (PVDF) polymers become popular in the use for flexible structure controlling. Applications of distributed piezoelectric sensors and actuators for active damping of beams and thin plates are investigated theoretically and verified experimentally by numerous researchers (cf Bailey and Hubbard, 1985; Clarc et al., 1991; Kapadia and Kawiecki, 1997; Chou

and Ho, 1998; among others). The applicable concepts of transverse motion control of a beam structure under moving inertial loads confirmed by experiments are reported by Bogacz and Popp (1997) and Frischgesell et al. (1999). An analysis of a system with bonded or embedded piezoelements is commonly based on a pure bending interaction of a perfectly bonded massless actuator (static approach) for both one dimensional and two dimensional piezoelectric effects (cf Bailey and Hubbard, 1985; Clarc et al., 1991; Dimitriadis et al., 1991; Tylikowski, 2000; Pietrzakowski, 2001a). The dynamic coupling model including the longitudinal motion of the actuator and a shear bonding layer is formulated by Tylikowski (1993) and developed and applied for the beam vibration control by Pietrzakowski (1997, 2001b) and Tylikowski (2001). The comparison of different models of the actuator/substructure interaction presented by Pietrzakowski (2000) shows that the static approximation is quite good for sufficiently thin piezoelectric patches, which are bonded to the main structure by stiff glue layers.

The presented study deals with the experimental investigation and theoretical analysis of a cantilever beam with the control system designed for active damping, which is composed of collocated piezoceramic sensors and actuators bonded to the beam surface. The basic mechanical and electrical parameters of the tested system have been identified. The experiments show that the beam transverse vibrations are reduced significantly by using the analog control circuit with velocity feedback. The experimental results of the active control of free and forced vibrations are compared with results of numerical simulations, which are performed using the static as well as dynamic model of the interaction between the piezoelectric actuator and the beam. In the case of steady-state vibrations the effects of the applied actuator/beam coupling models are demonstrated by means of the resonant curves corresponding to the first vibration mode.

2. Experimental setup

Experiments on active damping of vibration using a piezoelectric control system were conducted on a cantilever beam. The geometry of the tested beam is shown in Fig. 1.

The beam is constructed of a stainless steel strip of the length $l = 270\,\text{mm}$, width $b = 25\,\text{mm}$ and thickness $t_b = 1\,\text{mm}$, clamped at one end and free at the other. The clamped boundary conditions of the actual beam are confirmed measuring displacements at the point 2 mm far from the fastened edge. The

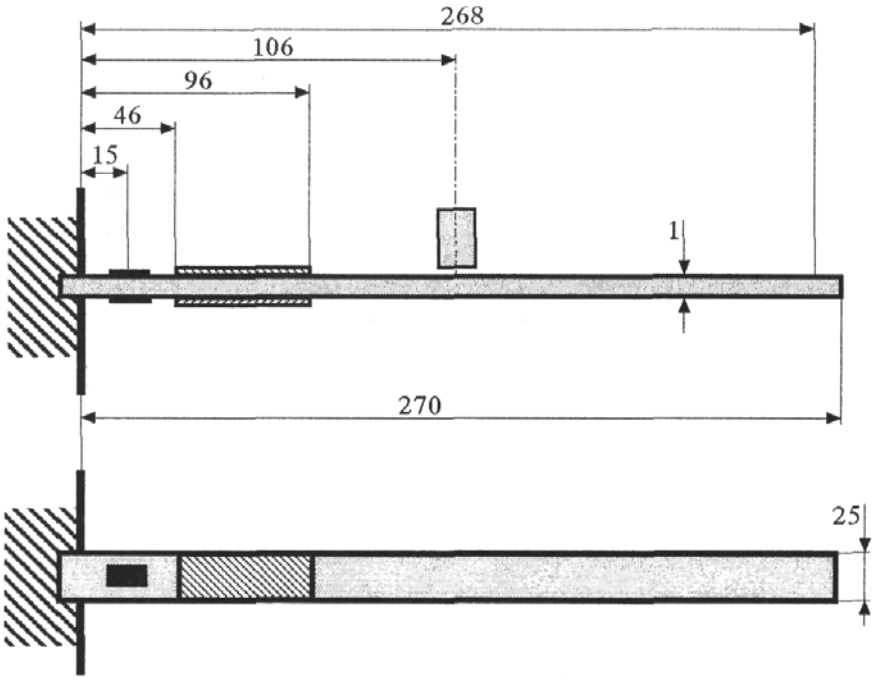

Fig. 1. Scheme of the tested beam

results are found less than 0.1% that of the tip-beam deflection. The sensor and actuator formed by a pair of piezoceramic patches are bonded on the opposite sides 46 mm from the root of the beam. A pair of "QickPack" piezoceramic transducers is used, QP10N type ($50.8 \times 25.4 \times 0.381$ mm) as the actuator and QP15N type ($50.8 \times 25.4 \times 0.254$ mm) as the sensor. They are attached to the beam surface using a two-part epoxy resin recommended for "QickPack" products.

The experimental investigation concerns suppression of the low frequency vibrations referred to the first-mode. The fundamental frequency of the beam specimen with the piezoceramic patches was measured to be $\omega_1 = 73.8\,1/\mathrm{s}$.

The control loop is composed using analog techniques. The signal from the piezoelectric sensor is fed to the pre-amplifier and then transformed by the derivative (D) controller due to the velocity feedback control strategy. Differentiation of the sensor signal introduces a time delay in the control system, which can be significant for higher natural frequencies. Therefore, filtering is necessary to remove high-frequency components of the control signal to avoid instability of the beam vibrations. The filter is installed between the pre-amplifier and the controller and is designed to eliminate any electrical signal with frequencies above $200\,1/\mathrm{s}$. The signal from the controller is finally amplified via the power amplifier and is then fed to the actuator to generate control action to suppress vibrations of the beam.

For the detection of the beam motion, a strain gauge system mounted near the clamped end is applied. The signal from the gauges working in a half bridge is sent to the measure amplifier (Spider 8 from HBM) with an analogue to digital (AD) converter installed and then recorded on a hard disk in a PC. The "Catman" data acquisition system is used for analyzing the data and visualizing the results.

The experimental setup for active control of the cantilever beam is shown in Fig. 2.

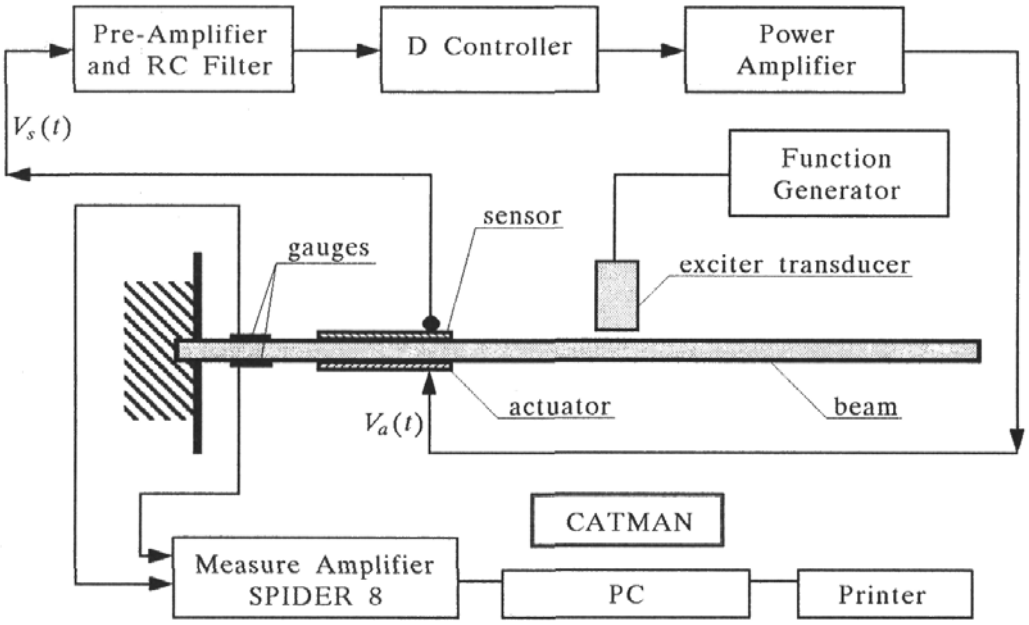

Fig. 2. Experimental setup

Experiments were performed for a harmonic excitation at a natural frequency and free vibrations of the beam; first without and then with the active control system. The transverse motion of the near-tip beam point at 2 mm from the free end is detected.

The steady-state vibrations of the beam are induced by the exciter transducer MM 0002 type (B&K) supplied by the function generator G 5010 (Ortel). For the distance between the transducer head and the beam surface recommended by the producer, the vibration amplitude depends mainly on the voltage applied to the exciter.

The time domain response of the beam excited at the first-mode natural frequency ($\omega_1 = 73.8\,1/\mathrm{s}$) without and with the control is presented in Fig. 3. This figure shows the histories of transient and steady-state vibrations after the control system was switched on with the gain $\kappa = 10$ (a) and the gain $\kappa = 25$ (b), respectively. The control gain κ is defined as a ratio of the

magnitude of the output voltage V_a applied to the actuator and the input voltage V_s generated by the sensor, $\kappa = V_a/V_s$. The improvement in reducing the amplitude of steady-state vibrations, which is measured as a ratio of the amplitudes without and with active damping, changes from 3.7 to 12.8 for the applied control gain values ($\kappa = 10$ and 25).

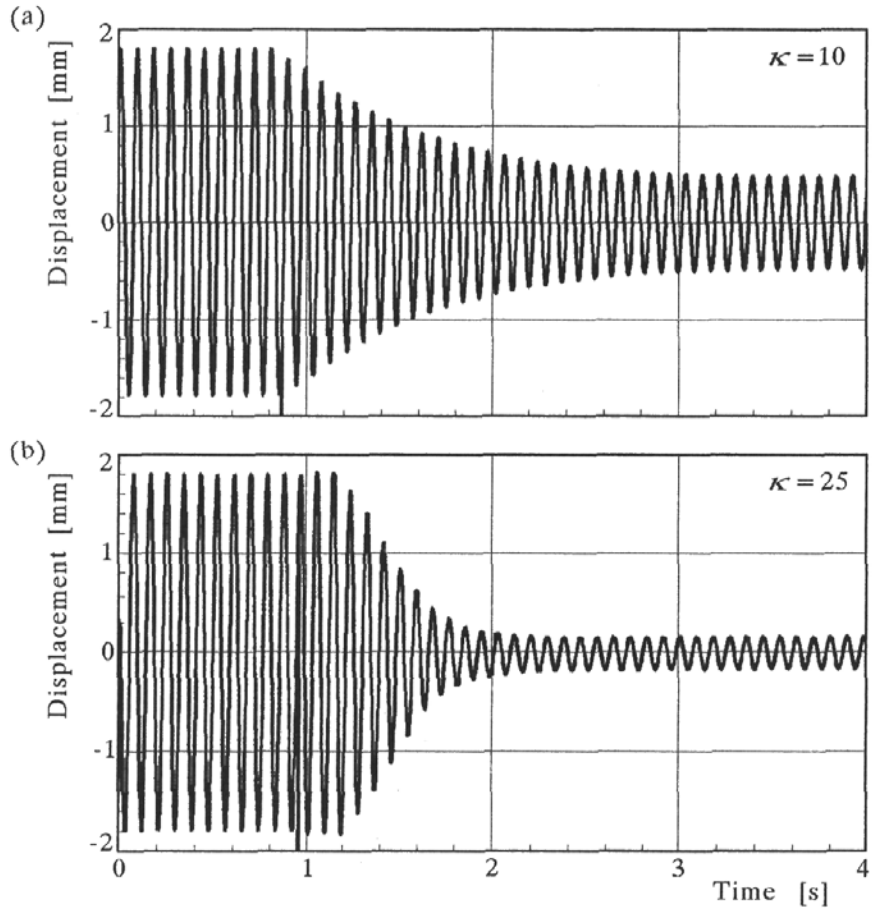

Fig. 3. Vibrations of the beam excited at the fundamental frequency without and with control (a) with gain $\kappa = 10$, (b) with gain $\kappa = 25$

To initiate free vibrations, the tip of the beam is deflected by about 3 mm and then released. The transient vibrations of the beam point represented the uncontrolled system and the actively damped beam with various control gains κ are shown in Fig. 4. It can be clearly noticed that the damping ratio increases significantly with increase in the control gain parameter. But the control system effectiveness is limited because of the high vibration modes, which are generated for sufficiently great values of the gain.

The passive suppression observed for the uncontrolled beam response (see Fig. 4, no control) is a combined effect due to material damping, air damping and damping created by the measuring and control equipment. The level of

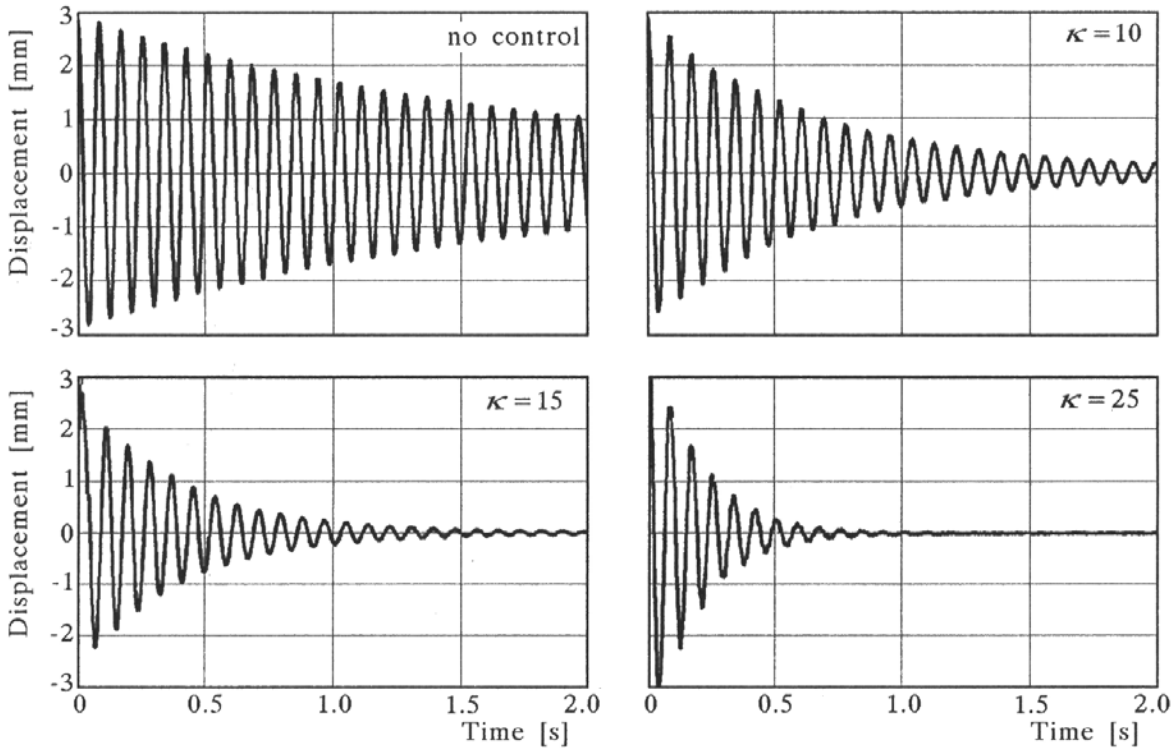

Fig. 4. Free vibrations of the beam without and with active damping. Effects of passive damping and variations in the control gain

the high frequency components is low even for the controlled vibrations, mainly due to the control signal filtering (low-pass filter installed in the control circuit). Therefore, the estimation of the damping coefficient, both for passive and active cases, can be based on the classical logarithmic decrement concept. The logarithmic decrement δ is expressed by the well-known relation

$$\delta = \frac{1}{i} \ln \frac{A_n}{A_{n+i}} \tag{2.1}$$

where A_n, A_{n+i} – free vibration amplitudes i periods apart.

Results of the logarithmic decrement calculations for passively damped transient vibrations are presented in Fig. 5.

The doted line is obtained for amplitudes recorded after one period $(i = 1)$. The differences between the values of the logarithmic decrement are caused by measurement errors and also by the influence of the second and higher modes on the beam response. The solid line refers to the averaged logarithmic decrement computed for a sequence of peaks 5 periods apart $(i = 5)$. Taking into account the locally averaged values and neglecting a slight tendency of their decreasing for lower amplitudes, the energy dissipation of the tested

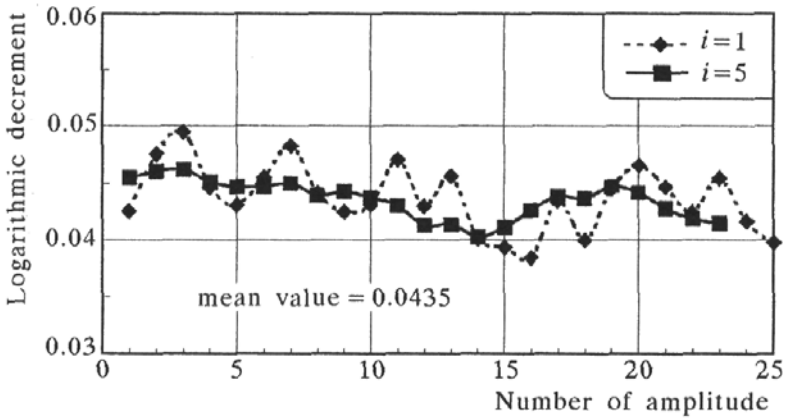

Fig. 5. Evaluation of passive damping

beam can be approximated by the equivalent logarithmic decrement of the value $\delta = 0.0435$.

The experimental results both for the excited and the free vibrations show that the active damping effect is evident. As expected, the intensity of reduction of the free vibration amplitude increases significantly for greater control gain parameters. A disadvantage of the used analog control system is an excitation of high vibration components observed for extremely great gain values.

3. Theoretical relations for the actively damped beam

3.1. Model of the actuator/beam interaction based on the idea of static relations

The dynamic analysis of the considered system can be simplified by imposing a pure bending model of the coupling between the beam and the perfectly bonded, massless piezoelement. Due to this model the actuator action caused by the applied voltage is reduced to bending moments at both ends of the piezoceramic patch. The transverse motion $w(x,t)$ of the controlled viscoelastic beam with a uniform bending stiffness and mass density, which is excited by the point force $F(t)$ can be described as follows

$$E_b J_b\Big(\frac{\partial^4 w}{\partial x^4} + \mu\frac{\partial^5 w}{\partial x^4 \partial t}\Big) + \rho_b b t_b \frac{\partial^2 w}{\partial t^2} = F(t)\delta(x - x_f) - \frac{\partial^2 M_a(x,t)}{\partial x^2} \tag{3.1}$$

where

E_b, ρ_b – beam Young's modulus and mass density, respectively

μ – viscous internal damping parameter of the Voigt-Kelvin model
J_b – cross-sectional moment of inertia
b, t_b – beam width and thickness, respectively
x_f – co-ordinate of the point force
$\delta(x)$ – Dirac function.

The bending moment $M_a(x,t)$ is distributed along the actuator and can be calculated taking into account the constitutive equation of the piezoelectric material and the moment equilibrium of the resultant forces acting in the cross-section of the beam (cf Bailey and Hubbard, 1985; Pietrzakowski, 2000; among others)

$$M_a(x,t) = C_a b_p(x) V_a(t) \tag{3.2}$$

where
$V_a(t)$ – voltage applied to the actuator
$b_p(x)$ – piezoelectric patch width described using the Heaviside function $b_p(x) = b[H(x-x_1) - H(x-x_2)]$
C_a – actuator constant given by the relation

$$C_a = \frac{d_{31}^a E_a E_b (t_b^2 + t_a t_b)}{2(E_b t_b + E_a t_a + E_s t_s)} \tag{3.3}$$

and
d_{31}^a – piezoelectric constant of the actuator
E_a, E_s – Young's moduli of the actuator and the sensor, respectively
t_a, t_s – thicknesses of the actuator and the sensor, respectively.

The input voltage $V_a(t)$ is generated by the piezoceramic sensor as a result of its deformation and then transformed via the controller due to the applied control function. Assuming the sensor strains to be the same as those of the beam surface, and after integrating the charge over the sensor electrode, the voltage produced by the sensor can be given as

$$V_s(t) = -C_s \int_0^l \frac{\partial^2 w}{\partial x^2} b_p(x)\, dx \tag{3.4}$$

where C_s is the sensor constant

$$C_s = d_{31}^s E_s \frac{t_b + t_s}{2C} \tag{3.5}$$

where
d_{31}^s – piezoelectric constant of the sensor
C – total sensor capacitance, $C = A_s e_{33}/t_s$
A_s – electrode area of the sensor
e_{33} – permittivity of the sensor material.

Assuming velocity feedback and after substituting Eq. (3.4), the control bending moment, Eq. (3.2), can be rewritten as follows

$$M_a(x,t) = k_d C_a C_s b_p(x) \int_0^l \frac{\partial^3 w}{\partial x^2 \partial t} b_p(x)\, dx \tag{3.6}$$

where k_d is the velocity gain factor of the controller.

The response of the actively damped beam subjected to a harmonic excitation can be expressed in terms of a transfer function. The block diagram with the velocity feedback is shown in Fig. 6.

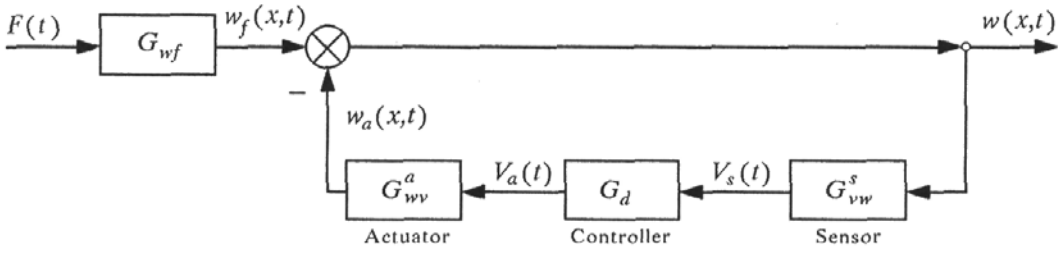

Fig. 6. Block diagram of the system

The steady-state solution to Eq. (3.1) can be written using the modal superposition

$$w(x,t) = \sum_{n=1}^{\infty} C_n W_n(x) \exp(\mathrm{i}\omega t) \tag{3.7}$$

where

C_n – amplitude coefficients
ω – frequency of the excitation
$W_n(x)$ – modal shape functions.

The modal functions are determined by the boundary conditions and for the cantilever beam of the length l having one end fixed and the other free are expressed in the well-known form

$$\begin{aligned} W_n(x) &= (\sin k_n l + \sinh k_n l)(\cosh k_n x - \cos k_n x) - \\ &- (\cos k_n l + \cosh k_n l)(\sinh k_n x - \sin k_n x) \end{aligned} \tag{3.8}$$

where k_n are the roots of the frequency equation $\cos k_n l \cosh k_n l = -1$ with the values of $k_n l = 1.875,\ 4.694,\ 7.855,\ldots,\ 0.5(2n-1)\pi$.

The transfer function G_{wf} relating the beam deflection to the loading force is given by the formula

$$G_{wf}(x,\omega) = \frac{w(x,\omega)}{F(\omega)} = \frac{1}{\rho_b b t_b} \sum_{n=1}^{\infty} \frac{W_n(x_f) W_n(x)}{\gamma_n^2(\omega_n^2 - \omega^2 + \mathrm{i}\mu\omega_n^2\omega)} \tag{3.9}$$

where ω_n is the nth natural frequency

$$\omega_n = k_n^2 \sqrt{\frac{E_b J_b}{\rho_b b t_b}} \tag{3.10}$$

and

$$\gamma_n^2 = \int_0^l W_n^2(x)\, dx$$

The transfer function of the output beam deflection to the input actuator voltage has the form

$$G_{wv}^a(x,\omega) = \frac{w(x,\omega)}{V_a(\omega)} = \frac{C_a}{\rho_b b t_b} \sum_{n=1}^{\infty} \frac{T_n W_n(x)}{\gamma_n^2(\omega_n^2 - \omega^2 + \mathrm{i}\mu\omega_n^2\omega)} \tag{3.11}$$

where T_n is the actuator shape factor

$$T_n = \int_0^l \frac{d^2 b_p(x)}{dx^2} W_n(x)\, dx = b\Big(\frac{dW_n(x)}{dx}\Big|_{x_2} - \frac{dW_n(x)}{dx}\Big|_{x_1}\Big) \tag{3.12}$$

The output voltage of the sensor caused by the beam deflection is given by the relation

$$G_{vw}^s(x,\omega) = \frac{V_s(\omega)}{w(x,\omega)} = \frac{G_{vf}^s(\omega)}{G_{wf}(x,\omega)} \tag{3.13}$$

where G_{vf}^s describes the response of the sensor voltage to the input external force and has the form

$$G_{vf}^s(\omega) = \frac{V_s(\omega)}{F(\omega)} = \frac{C_s}{\rho_b b t_b} \sum_{n=1}^{\infty} \frac{S_n W_n(x_f)}{\gamma_n^2(\omega_n^2 - \omega^2 + \mathrm{i}\mu\omega_n^2\omega)} \tag{3.14}$$

where S_n is the sensor shape factor

$$S_n = \int_0^l \frac{d^2 W_n(x)}{dx^2} b_p(x)\, dx \tag{3.15}$$

Considering the velocity feedback, the controller transforms the input voltage signal according to the transfer function

$$G_d(\omega) = \mathrm{i}k_d\omega \tag{3.16}$$

where k_d is the derivative gain factor.

The closed-loop transfer function of the controlled beam is given by the well-known equation

$$G_c = \frac{G_{wf}}{1 + G_o} \tag{3.17}$$

where G_o is the open-loop transfer function defined as the following product

$$G_o = G^s_{vw} G_d G^a_{wv} \tag{3.18}$$

Free vibrations of the beam can be analysed using the impulse transfer function. The time-response of the system to the impact $F(t) = \delta(t)$ is defined as the inverse Fourier transform of the transfer function $G_c(x, \omega)$

$$h_c(x,t) = \frac{1}{2\pi} \int_{-\infty}^{\infty} G_c(x,\omega) \exp(\mathrm{i}\omega t)\, d\omega \tag{3.19}$$

The model of the system based on the static coupling concept can be modified by dividing the beam into segments due to its geometry. In this case the activated section is treated as a laminated beam composed of mechanically isotropic layers. Hence, the bending stiffness $E_b J_b$ can be replaced by the equivalent stiffness $\overline{EJ}$ defined as follows

$$\overline{EJ} = \sum_{k=1}^{3} E_k J_k \tag{3.20}$$

where

E_k – Young's modulus of the kth layer

J_k – cross-sectional moment of inertia of the kth layer relative to the midplane.

The governing equations for the beam sections can be written in the form:

— for the activated sections

$$\overline{EJ}\Big(\frac{\partial^4 w}{\partial x^4} + \mu \frac{\partial^5 w}{\partial x^4 \partial t}\Big) + \overline{\rho} b t_b \frac{\partial^2 w}{\partial t^2} = 0 \tag{3.21}$$

— for the classical beam sections

$$E_b J_b \Big(\frac{\partial^4 w}{\partial x^4} + \mu \frac{\partial^5 w}{\partial x^4 \partial t}\Big) + \rho_b b t_b \frac{\partial^2 w}{\partial t^2} = 0 \tag{3.22}$$

where $\overline{\rho}$ denotes the equivalent density of the activated section

$$\overline{\rho} = \frac{\rho_b t_b + \rho_p(t_a + t_s)}{t_b}$$

with ρ_p being the density of the piezoelectric elements.

The boundary conditions corresponding to the clamped-free ends and the continuity conditions between particular sections of the beam can be written as the following system of equations

$$\begin{aligned}
&w(0,t) = \frac{\partial w}{\partial x}\Big|_{x=0} = 0 \qquad \frac{\partial^2 w}{\partial x^2}\Big|_{x=l} = \frac{\partial^3 w}{\partial x^3}\Big|_{x=l} = 0 \\
&w(x_f^-,t) = w(x_f^+,t) \qquad w(x_1^-,t) = w(x_1^+,t) \qquad w(x_2^-,t) = w(x_2^+,t) \\
&\frac{\partial w}{\partial x}\Big|_{x_f^-} = \frac{\partial w}{\partial x}\Big|_{x_f^+} \qquad \frac{\partial w}{\partial x}\Big|_{x_1^-} = \frac{\partial w}{\partial x}\Big|_{x_1^+} \qquad \frac{\partial w}{\partial x}\Big|_{x_2^-} = \frac{\partial w}{\partial x}\Big|_{x_2^+} \\
&M(x_f^-,t) = M(x_f^+,t) \qquad M(x_1^-,t) = M(x_1^+,t) \qquad M(x_2^-,t) = M(x_2^+,t) \\
&T(x_f^-,t) = T(x_f^+,t) \qquad T(x_1^-,t) = T(x_1^+,t) \qquad T(x_2^-,t) = T(x_2^+,t)
\end{aligned} \tag{3.23}$$

It should be noticed that the continuity of the bending moment between the activated and classical beam sections ($x = x_1$ and x_2) yields

$$\begin{aligned}
&\frac{\partial^2 w}{\partial x^2}\Big|_{x_1^-} = \frac{\overline{EJ}}{EJ}\frac{\partial^2 w}{\partial x^2}\Big|_{x_1^+} + \frac{M_a}{EJ} \\
&\frac{\overline{EJ}}{EJ}\frac{\partial^2 w}{\partial x^2}\Big|_{x_2^-} + \frac{M_a}{EJ} = \frac{\partial^2 w}{\partial x^2}\Big|_{x_2^+}
\end{aligned} \tag{3.24}$$

The continuity of the transverse force in the cross-section $x = x_f$, where the point force $F(t)$ is applied, is given by the relation

$$\frac{\partial^3 w}{\partial x^3}\Big|_{x_f^-} = \frac{\partial^3 w}{\partial x^3}\Big|_{x_f^+} + \frac{F}{E_b J_b} \tag{3.25}$$

The governing equations, the boundary and continuity conditions state the boundary value problem.

3.2. Model of the system based on the dynamic concept of the actuator/beam interaction

The advanced model of the system is formulated on the consideration of an elastic bonding layer between the actuator and the beam. Assuming the

actuator extension with inertia forces and the one-dimensional shearing effect in the bonding interlayer the dynamic relations are obtained for particular sections of the beam (cf Tylikowski, 1993; Pietrzakowski, 1997, 2001b).

The motion of the activated section is described by two coupled equations expressed in the beam transverse displacement $w(x,t)$ and the pure longitudinal displacement $u_a(x,t)$ of the actuator

$$E_b J_b\Big(\frac{\partial^4 w}{\partial x^4} + \mu\frac{\partial^5 w}{\partial x^4 \partial t}\Big) + \overline{\rho} b t_b \frac{\partial^2 w}{\partial t^2} - \frac{\kappa_g b t_b}{2}\frac{\partial}{\partial x}\Big(u_a + \frac{t_b}{2}\frac{\partial w}{\partial x}\Big) = 0$$
$$E_a t_a \frac{\partial^2 u_a}{\partial x^2} - \rho_p t_a \frac{\partial^2 u_a}{\partial t^2} - \kappa_g\Big(u_a + \frac{t_b}{2}\frac{\partial w}{\partial x}\Big) = 0 \tag{3.26}$$

where κ_g is the shearing factor defined as the ratio of the shear modulus and thickness of the glue interlayer, $\kappa_g = G/t_g$.

The motion of other beam sections is given by the Bernoulli-Euler equation for viscoelastic beam, Eq. (3.22).

The equations of motion have to satisfy the above mentioned boundary conditions of the cantilever beam at $x = 0$ and $x = l$, continuity of the beam deflection, slope, curvature and transverse force at the borders of the sections, and also the free stress condition for the ends of the actuator. The continuity of the transverse force at the actuator border co-ordinates x_1 and x_2 should be obtained taking into account the shear stresses transmitted through the bonding layer. For example, the above relation at x_1 can be expressed by the equation

$$E_b J_b \frac{\partial^3 w}{\partial x^3}\Big|_{x_1^-} = E_b J_b \frac{\partial^3 w}{\partial x^3}\Big|_{x_1^+} - \frac{\kappa_g b t_b}{2}(u_a - u_b)\Big|_{x_1^+} \tag{3.27}$$

where u_b is the beam surface longitudinal displacement

$$u_b = -\frac{t_b}{2}\frac{\partial w}{\partial x}$$

The free stress condition at the actuator borders is based on the stress-strain relation $\sigma_a = E_a(\varepsilon_a - \lambda)$ and has the form

$$\varepsilon_a(x_j) = \frac{\partial u_a}{\partial x}\Big|_{x_j} = \lambda \qquad j = 1,2 \tag{3.28}$$

where the actuator strain λ is given by the strain-voltage relation characteristic for the piezoelectric material

$$\lambda = \frac{d_{31}^a}{t_a} V_a \tag{3.29}$$

The voltage V_a supplying the actuator is proportional to the time derivative of the voltage generated by the sensor, according to the feedback rule.

Assuming the harmonic loading force, $F(t) = F_0 \exp(\mathrm{i}\omega t)$, the steady-state solutions to the dynamic equations can be written as

$$w(x,t) = W(x)\exp(\mathrm{i}\omega t)$$
$$u_a(x,t) = U_a(x)\exp(\mathrm{i}\omega t) \tag{3.30}$$

The displacement distributions $W(x)$ within the beam sections and $U_a(x)$ along the actuator are obtained by solving the boundary value problem formulated by the governing equations and the boundary conditions. These spatial functions determined for every frequency ω enable calculation of the frequency characteristics of the transverse displacements of the beam controlled by the piezoelectric system.

4. Results of simulation

The numerical simulation was performed for a model of the system whose geometry is described in Section 2. It is assumed that the Young modulus of the stainless steel beam is $E_b = 2.05{\cdot}10^{11}\ \mathrm{N/m^2}$. The material viscous damping (Voigt-Kelvin model) is calculated for free vibrations of the tested beam due to the relation $\mu = \delta/(\pi\omega_1)$. Substituting the fundamental frequency $\omega_1 = 73.8\ 1/\mathrm{s}$ and the equivalent logarithmic decrement $\delta = 0.0435$, the damping parameter is estimated to be $\mu = 1.88 \cdot 10^{-4}\ \mathrm{s}$.

Applying the simple static coupling model with the constant stiffness and mass density along the beam (Section 3.1), the Young modulus is derived to be $E_b = 2.19 \cdot 10^{11}\ \mathrm{N/m^2}$ in order to match the theoretical first natural frequency of the beam with the measured one. The increase of the beam stiffness is justified because of the local stiffening effect of the piezoceramic patches.

The electro-mechanical parameters of the piezoceramic transducers are determined basing on the technical data given in "QickPack piezoelectric actuators" (1997). The equivalent Young modulus of the actuator and sensor patches are calculated applying the mixture rule for the piezoceramic PZT material with $E_p = 6.3{\cdot}10^{10}\ \mathrm{N/m^2}$ and the resin covering with $E_m = 2.8{\cdot}10^{9}\ \mathrm{N/m^2}$. The piezoelectric coefficient d_{31} refers to the linear estimation of the strain-voltage characteristic of the piezoceramic devices for voltage amplitudes less than 60 V. The electro-mechanical parameters used in calculations are listed in Table 1.

Table 1. Material parameters of transducers

Material parameter	Actuator QP10N	Sensor QP15N
ρ [kg/m^3]	5780	6900
E [N/m^2]	$3.3 \cdot 10^{10}$	$2.5 \cdot 10^{9}$
d_{31} [m/V] or [C/N]	$2.3 \cdot 10^{-10}$	$2.5 \cdot 10^{-10}$
C [μF]	0.06	0.10

The amplitude-frequency characteristics at the first mode region depending on the applied model of the system are shown in Fig. 7. The dynamic responses are calculated at the measure point ($x = 268$ mm). The amplitude of resonant vibrations for the uncontrolled beam is determined by matching it with the measured amplitude of the steady-state vibrations presented in Fig. 3. The frequency response of the actively damped beam is obtained assuming the derivative gain factor $k_d = 0.135$ s, which for the fundamental frequency ω_1 refers to the control-loop gain $\kappa = 10$ due to the relation $\kappa = \omega_1 k_d$. For the applied models of the system the ratios of the uncontrolled and the actively damped resonant amplitudes are close to the measured ones. The amplitude reduction is almost the same as that of the experimental result (about 3.4 times) when the segmented beam with the static coupling model is used. By comparing the plots, it can be noticed that the characteristics become slimmer and the control effectiveness decreases for more comprehensive models of the system. These effects are clearly exposed for the dynamic coupling model with a bonding layer. Even a relatively high value of the shearing stiffness parameter $\kappa_g = 5 \cdot 10^{12}$ N/m^3 cannot improve the active damping ratio enough because of the dynamic interaction of the actuator.

To obtain free vibrations, the beam end is subjected to an impulse excitation. The beam response is calculated according to Eq. (3.19) derived for the simplified model. For comparison of the simulation and experimental results the impulse value is determined by matching the beginning response amplitudes with the initial displacement of the tested beam. The results of simulation obtained for the uncontrolled system and for several values of the gain factor $k_d = 0.135$ s ($\kappa = 10$), $k_d = 0.203$ s ($\kappa = 15$), $k_d = 0.338$ s ($\kappa = 25$) are presented in Fig. 8.

As mentioned above, the passive damping refers to the Voigt-Kelvin model with the retardation time $\mu = 1.88 \cdot 10^{-4}$ s, which quite well describes the energy dissipation of the tested beam (compare the time histories for the uncontrolled beam, Fig. 8 and Fig. 4). In the plots corresponding to the actively damped beam the effect of the gain factor increasing is obvious. The compari-

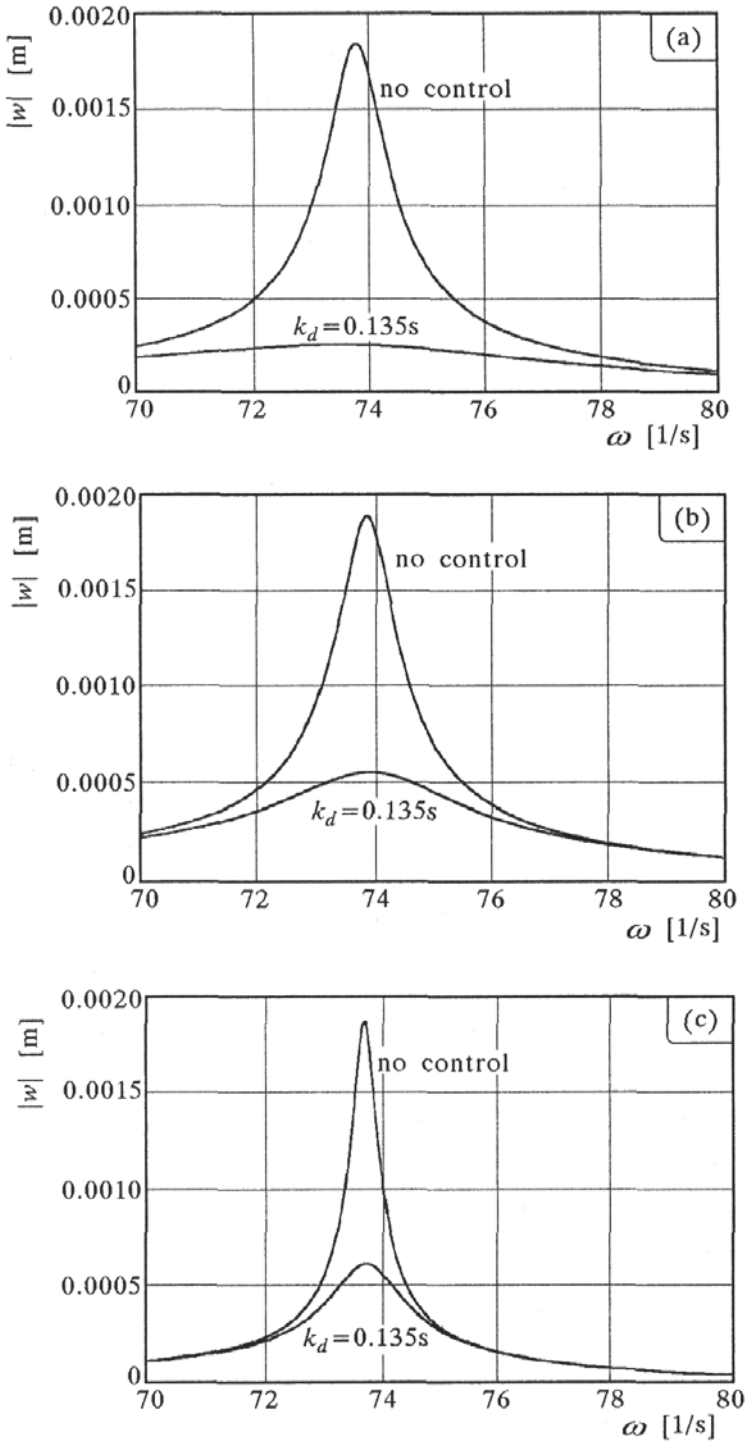

Fig. 7. Active damping effect depending on the model of the system; (a) static coupling model with a constant beam stiffness, (b) static coupling model with the segmented beam, (c) dynamic coupling model

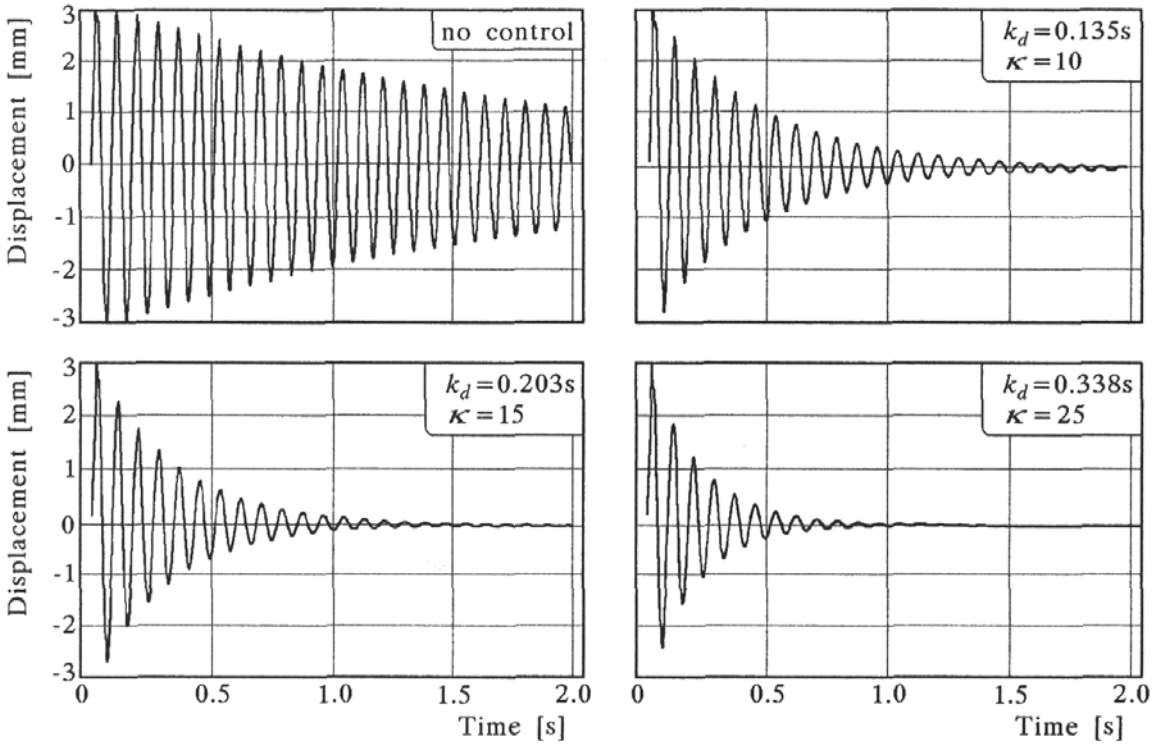

Fig. 8. Impulse response for the beam simplified model without and with active damping. Effects of passive damping and variation in the control gain

son of the results of simulation and the free vibration time histories obtained experimentally leads to the conclusion that the active damping effectiveness is generally similar but it is noticeably greater for the theoretical evaluation with the lower control gain values $\kappa = 10$ and 15. The reason for this behaviour can be the applied simple model of the system with the additional stiffness of the activated segment neglected and the perfect bonding assumed. As shown in the case of steady-state vibrations (Fig. 7) the performance of active damping depends, among others, on the bonding layer parameters and shear strains in the layer (cf Pietrzakowski, 2001b).

The influence of the control gain factor on the logarithmic decrement within the applicable range of the control gain values for both the experiment and the simulation is demonstrated in Fig. 9. Each indicated point of the plots refers to the mean logarithmic decrement calculated for the sequential amplitudes 1 period apart. The number of recorded peaks varied from 5 to 15 for the high and low control gains, respectively. As expected, the logarithmic decrement is a linear function of the gain for the considered theoretical model of the system. The curve related to the experiment shows that the damping intensity increases slightly for low and extremely high control gains. Within

the applicable gain range, the logarithmic decrement of the tested beam is generally less than its theoretical approximation except for the relatively high gain values ($\kappa = 20 \div 25$). The discussed relation results not only from the mechanical behaviour of the real system but also from the electrical properties of the control loop with the analog devices.

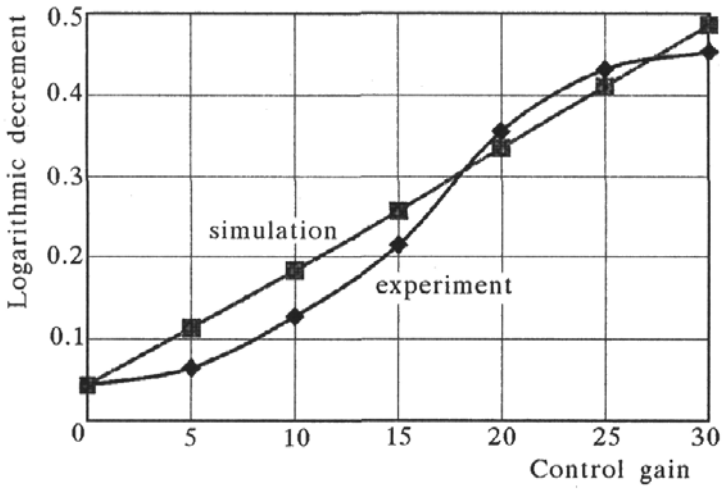

Fig. 9. Logarithmic decrement versus control gain for the experimental and numerical simulation

5. Final remarks

The active damping technique using piezoceramic sensors and actuators was demonstrated by the experiment and described theoretically. The investigation was focused on suppression of low frequency vibrations of a cantilever beam. The experimental results of free as well as forced vibrations confirmed that even a simple analog feedback with the derivative controller is effective for the active damping of the beam transverse motion. Increasing the gain of the control circuit the vibration amplitude reduction can be significantly increased. In practice, the gain values are limited because of the tendency of the control system to amplify unwanted high vibration components. The simulation results showed a quite good agreement with the experiment even for the simplified model of the controlled beam. The model quality can be improved by taking into account the local stiffening of the activated beam. Considering the dynamic model of the interaction between the actuator and the beam the influence of the bonding layer properties on the control effectiveness was pointed out.

References

1. BAILEY T., HUBBARD J.E., 1985, Distributed piezoelectric-polymer active vibration control of a cantilever beam, *Journal of Guidance, Control and Dynamics*, **8**, 605-611

2. BOGACZ R., POPP K., 1997, Theoretical analysis and experimental verification controlled beam structure under moving inertial loads, *Proceedings of Third Intern. School on Active Methods of Reduction of Vibrations and Noise*, Kraków-Zakopane, 33-38

3. CLARC R.L., FULLER CH.R., WICKS A., 1991, Characterization of Multiple Piezoelectric Actuators for Structural Excitation, *J. Acoust. Soc. Am.*, **90**, 346-357

4. CHOU C.S., HO C.D., 1998, Control of vibration of a base excited beam, *Proceedings of SPIE Conference Mathematics and Control in Smart Structures*, **3323**, 382-392

5. DIMITRIADIS E., FULLER C.R., ROGERS C.A., 1991, Piezoelectric actuators for distributed vibration excitation of thin plates, *Journal of Applied Mechanics*, **113**, 100-107

6. FRISCHGESELL T., KRZYŻYŃSKI T., BOGACZ R., POPP K., 1999, Dynamics and control of a guideaway under a moving mass, *Int. Journal Vehicle Design*, 176-189

7. KAPADIA R.K., KAWIECKI G., 1997, Experimental evaluation of segmented active constrained layer damping treatments, *Journal of Intelligent Material Systems and Structures*, **8**, 103-111

8. PIETRZAKOWSKI M., 1997, Dynamic model of beam-piezoceramic actuator coupling for active vibration control, *Journal of Theoretical and Applied Mechanics*, **35**, 3-20

9. PIETRZAKOWSKI M., 2000, Multiple piezoceramic segments in structural vibration control, *Journal of Theoretical and Applied Mechanics*, **38**, 35-50

10. PIETRZAKOWSKI M., 2001a, Active damping of laminated plates by skewed piezoelectric patches, *Journal of Theoretical and Applied Mechanics*, **39**, 377-393

11. PIETRZAKOWSKI M., 2001b, Active damping of beams by piezoelectric system: effects of bonding layer properties, *International Journal of Solids and Structures*, **38**, 7885-7897

12. TYLIKOWSKI A., 1993, Stabilization of beam parametric vibrations, *Journal of Theoretical and Applied Mechanics*, **31**, 3, 657-670

13. TYLIKOWSKI A., 2000, Two-dimensional piezoelectric actuators for vibration excitation and suppression of thin plates, *Machine Dynamics Problems*, **24**, 199-207

14. TYLIKOWSKI A., 2001, Effects of piezoactuator delamination on the transfer functions of vibration control systems, *International Journal of Solids and Structures*, **38**, 2189-2202

15. QickPack piezoelectric actuators. Active Control eXperts, Inc., 1997

Badania doświadczalne i symulacyjne sterowania drganiami belki wspornikowej

Streszczenie

W pracy przedstawiono rezultaty badań doświadczalnych i symulacyjnych aktywnego tłumienia poprzecznych drgań belki wspornikowej. Zastosowany układ sterowania składa się z piezoceramicznych elementów tworzących parę pomiarowo-wykonawczą, połączonych pętlą prędkościowego sprzężenia zwrotnego. Wyniki eksperymentu, dotyczące zarówno drgań swobodnych, jak i drgań wymuszonych w zakresie niskich częstości, potwierdzają skuteczność układu sterowania z analogowym regulatorem różniczkującym. W celu weryfikacji teoretycznych modeli badanego układu przeprowadzono symulację numeryczną. W ramach analizy wprowadzono uproszczony model układu mechanicznego (podejście statyczne), w którym oddziaływanie elementu wykonawczego idealnie połączonego z belką ograniczono do czystego zginania, przyjmując belkę o stałej zastępczej sztywności lub belkę lokalnie usztywnioną przez naklejone elementy piezoelektryczne. W zastosowanym dynamicznym modelu połączenia uwzględniono bezwładność elementu wykonawczego działającego na belkę za pośrednictwem warstwy kleju o skończonej sztywności na ścinanie. Wyniki symulacji dość dobrze pokrywają się z wynikami uzyskanymi na drodze doświadczalnej także w przypadku uproszczonego modelu układu. Uwzględnienie w obliczeniach warstwy kleju oraz wzdłużnego ruchu elementu wykonawczego powoduje obniżenie skuteczności aktywnego tłumienia nawet dla warstw o stosunkowo dużej sztywności.

Manuscript received November 13, 2001; accepted for print March 4, 2002